Decomposition of the Hot-Spot Factor

Zoran Radaković, Uroš Radoman, and Predrag Kostić

***Abstract*—This paper describes the application of the finite-elements method for determining the distribution of losses over windings and a detailed thermal-hydraulic network model for determining the value of the hot-spot factor and the hot-spot temperature. The influence of nonuniform losses in the conductor of the windings and the influence of nonuniform cooling are clearly separated. A detailed discussion of the components included in the hot-spot factor is given in this paper, enabling proper understanding of this complex and important quantity. The case study transformer was a 100-MVA oil power transformer with oil-directed water-forced cooling. The method was applied within the scope of the project of increasing the power of a hydro power station by 12%. The task was to calculate the temperatures and to recommend whether the reconstruction of the transformer is necessary. The developed calculation method and software were hitherto used for transformer design (in the production or the reconstruction stage of transformers) and it is the first application to give an answer as to whether it is possible to increase the power of an existing transformer. In this specific application, necessary onsite measurements for determining the characteristics of the coolers were performed.**

***Index Terms*—Hot spot, loading, oil power transformer, thermal design, thermal-hydraulic network model.**

I. Introduction

A HOT-SPOT insulation temperature and the hottest oil temperature are calculated in the process of transformer design [1]. These temperatures must be below the allowed limits for the applied type of oil and solid insulation. There are standards related to heat-run tests, as a part of transformer acceptance tests [2] and standards specifying the temperature limits during transformer operation [3].

The practical problem initiating this study was a project to increase the power of a hydropower plant by 12%, while the transformer should operate at a lower voltage (90% of the rated voltage); thus, the increase in the current with respect to the rated one amounts to 24.4% ((112/100)/0.9=1.244). A current increase of 24.4% would cause an increase of the winding losses of ca. 54.8% (1.244^2-1), leading to an increase in the oil and winding temperatures. An important fact is that this transformer, as many other transformers in operation [4], is oversized, that is, the real rated power is higher than the declared one (100 MVA); the real rated power is the one at which one of three characteristic temperatures (hot-spot, top oil, or average winding) reaches its allowed limit. Transformer oversizing is dominantly a consequence of the introduction of high safety margins due to limited accuracy of the methods for thermal calculations (the statistics of the oversizing of large transformers, based on a large number of heat-run tests, is given in [4]).

These days, a detailed thermal-hydraulic network model (THNM) is widely seen by experts as the base on which thermal design tools should be established. The basics of a detailed THNM are presented in [5]; in publications following this one (for example, in [6] and [7]), we presented practical applications of software developed based on this model; some relevant papers by the other authors are [8] and [9]. The basic relevant text books, handbooks, and papers are [10]–[13]. The results of recent research of relevant hydraulic and thermal details, based on experiments and usage of finite-elements tools, are published in [14]–[16].

In the present study, a detailed thermal-hydraulic model and the corresponding software written in C# were applied to perform the thermal calculation of the transformer on increased load and losses, and to check whether the hot-spot and maximum oil temperatures exceed the allowed values. Prior to these thermal calculations, finite-element calculations were performed to determine the distribution of the losses over the windings, that is, the losses in each conductor.

For the application of the detailed THNM, it was necessary to identify the characteristics of the oil/water cooler. The considered transformer was built in 1989, and there are no available standard catalog data about the cooler. For this reason, as a first step, measurements were made on the transformer during real operation to determine the required data.

In addition to the consideration of the practical issue, if the planned increase of the transformer current load is acceptable, this paper would also contribute to a better understanding of the hot-spot factor.

II. Power Losses

A. Losses Measured in the Factory Acceptance Test

Losses obtained from 100-MVA (three-phase, Yd5, 242/15.65-kV, short-circuit impedance 11.95%) power transformer factory acceptance tests were the following: no-load losses at the rated voltage U_r : $P_{Fer} = 63.8$ kW, no-load losses at 0.9 U_r: $P_{Fe0.9} = 46.4$ kW, short-circuit losses at the rated current recalculated to 75°C: $P_{Cur} = 319.8$ kW.

B. Distribution of Core Losses

Input data for the software are values of losses in following parts of the core: limbs, yokes above/below limb, and yokes between limbs. Since the cross sections of the limbs and the yokes are similar, the distribution of core losses over parts of the

Manuscript received February 24, 2014; revised May 20, 2014 and July 30, 2014; accepted August 21, 2014. Date of publication September 16, 2014; date of current version January 21, 2015. Paper no. TPWRD-00213-2014.

The authors are with of the Faculty of Electrical Engineering, University of Belgrade, Belgrade 11000, Serbia (e-mail: radakovic@etf.rs).

Digital Object Identifier 10.1109/TPWRD.2014.2352039

core was estimated according to the lengths of the parts. These losses at the rated voltage are: limb 9810 W, yoke above/below limb 3550 W, and yoke between limbs 3270 W. At 90% of the rated voltage, the losses in each part are 27.3% smaller (the ratio of total core losses amounts to 46.4/63.8).

C. Losses in the Windings

1) Methodology: The 2-D magnetic-field distribution in the low-voltage (LV) and high-voltage (HV) windings (axial and radial components) was calculated using finite-elements (FEM) software [17], [18]. The input data to FEM were the shape of the three-limb core, exact position of each conductor in both windings (HV and LV) of each of the three limbs, the electric connections of parts of the windings, and the direction of the turns.

The magnetic field is different in the zone where the winding is between the yokes (window plane) and in the zone where there is a free space below and above the windings (plain perpendicular to window); for this reason, a 2-D FEM calculation was made of all three phases in the central core plane.

Eddy losses per-unit volume $p_e = p_{ex} + p_{ey}(\mathrm{W/m^3})$ are calculated from the calculated distribution of the magnetic field as [19]

$$p_{\mathrm{ex}} = \frac{\omega^2 B_x^2 (\mathrm{dim}Y)^2}{24\rho} \tag{1}$$

$$p_{\mathrm{ey}} = \frac{\omega^2 B_y^2 (\mathrm{dim}X)^2}{24\rho} \tag{2}$$

where ω is the angular frequency ($\omega = 2\pi f$, where f is the frequency), B_x and B_y are the radial and axial components of the leakage flux density vector, ρ is the electrical resistivity, and $dimX$ and $dimY$ are the width and height of the conductor. These are approximate equations, valid for the case when the dimensions of the conductor are small compared to the depth of penetration (for copper (58.14 Sm/mm^2 and for a 50-Hz frequency: the depth of penetration is equal to 9.33 mm). From this point of view, the accuracy of the calculation of the losses, especially due to B_x at the bottom and the top of the winding, could be improved. At this point, the state of the art of the tools used these days in transformer engineering was retained; the results of the present calculation method were compared with the results of nine methods used by large transformer producer companies and other official software (the strand of the case transformer was 2.057 × 14.275 mm) [20] and the obtained results were very similar to the average value of these nine methods. For a temperature of 75 °C, the electrical resistivity amounts to $\rho = \rho_{20}(235 + 75)/(235 + 20) = 2.04210^{-8}$ Ωm ($\rho_{20} = 1.68 \cdot 10^{-8}$ Ωm). Two values of p_e were calculated—based on the results of the FEM calculations of the magnetic field, for the space between two limbs and for the space outside the outer limb. The leakage field distribution is generally affected by the transformer geometry and the location of magnetic shunts. By considering this, the calculation accuracy would be improved. The product of p_e between the yokes with the volume of a turn quarter will be denoted as P_Y and the same product of p_e free space below and above the windings will be denoted as P_F.

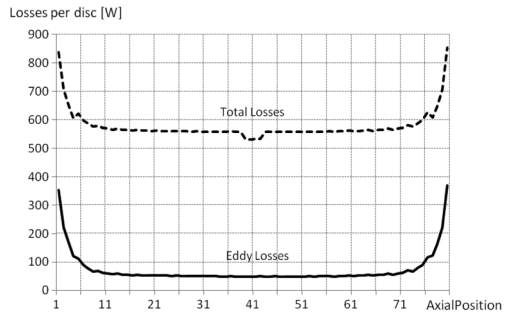

Fig. 1. Rated losses per disc in the HV winding.

The eddy losses in each conductor are determined as 4 times the average value of the losses in the conductors quarters: $4(4P_Y + 8P_F)/12 = (4P_Y + 8P_F)/3$ (there are 4 conductor quarters (2 × 1 (end phases) +1 × 2 (middle phases)) with P_Y and 8 conductor quarters [2 × 3 (end phases) +1 × 2 (middle phases)] with P_F; it is assumed that the field in the plane perpendicular to the window and the field in the space outside the outer limbs of the window plane are equal).

The HV winding is coiled from the middle of the winding as two parallel coils, each consisting of 6 discs with 21 flat rectangular conductors (copper 16.1 × 3.2 mm, thickness of the paper insulation on both sides 1.8 mm) and 34 discs with 22 flat rectangular conductors (also 16.1 × 3.2 mm).

The LV winding is coiled as a two-layered double helix (two helices in parallel) with 49 electrical turns each (50 mechanical; one additional mechanical turn is the consequence of the transposition of the continuously transposed conductor (CTC) strands). Each conductor is CTC (both side thickness of the paper insulation is 0.6 mm, and both side thickness of the enamel is 0.05 mm; outer conductor size is 14.65 × 38.5 mm), and consists of 10 separated rectangular strands (copper 14 × 3.2 mm). The entry current was assumed to be equally divided between the two parallel branches, each of them dividing into 10 parallel strands.

The total losses per-unit volume in each conductor are equal to the sum of the eddy losses, described before, and the dc losses. DC losses per unit volume were calculated as the simple product of current density squared and the resistivity ρ.

2) Results: Fig. 1. shows the rated losses in each of the 80 discs along the height of the HV winding. Fig. 2 shows the distribution of losses over the conductors of discs in the radial direction in seven typical discs (the top five, where higher losses due to the radial component of the magnetic field appear, the 10th from the top and the 20th from the top; losses in discs 20–40 from the top were almost the same and the losses were quite symmetrical with respect to the axial distance from the middle of the winding).

The distribution of total losses in the LV winding over height (there is only one conductor in the radial direction), presented in Fig. 3, is of a similar shape as the distribution given per disc in Fig. 1. The dc losses per conductor amount to 139.9 W in the inner layer, and 158.4 W in the outer layer. The losses in each

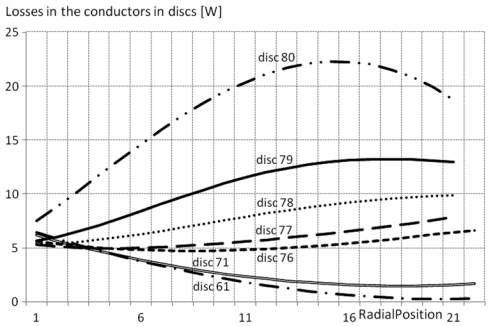

Fig. 2. Rated eddy losses per conductor in the HV winding.

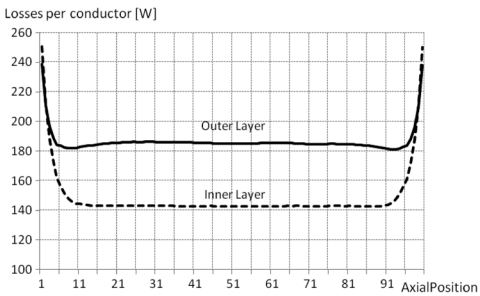

Fig. 3. Rated total losses per conductor in the LV winding.

conductor were calculated as the sum of the losses in each of the 10 CTC strands, determined by the FEM software.

D. Losses in the Constructive Parts

Total losses in each winding ($P_{\gamma LV}$ and $P_{\gamma HV}$) were calculated as the sum of the dc losses and the eddy losses in each conductor. Rated losses in constructive parts (P_{Constr}) were equal to the value of losses measured in the factory short-circuit test ($P_{\mathrm{SC}} = 319807$ W) minus the losses in the windings ($P_{\mathrm{Constr}} = P_{\mathrm{SC}} - 3(P_{\gamma LV} + P_{\gamma HV})$; $P_{\gamma LV} = 33553$ W, and $P_{\gamma HV} = 46250$ W). The obtained value of 80398 W ≈80 kW is divided in the following way: in tank surfaces (20 kW in each of longer walls, 8 kW in each of shorter walls, 8 kW in the cover, and 8 kW in the floor), in a constructive part below the windings (4 kW) and in the constructive part above the windings (4 kW). This distribution does not significantly affect the final results of the thermal calculations and, for this reason, it was possible to roughly estimate it.

For the increased current load (1.244 p.u.), the losses in the constructive parts are increased $1.244^2 \approx 1.5$ times with respect to the corresponding losses under the rated load (the total value of losses in constructive parts under the increased load are 120 kW).

E. Overview of the Total Losses Under the Rated and Planned Increased Load

The losses in the LV and HV windings (under the assumption that the temperature is uniform and equal to 75 °C), in the core and in the constructive parts are (the first number is for the regime with the rated power and rated voltage and the second is for the regime with the power increased by 12% and a voltage equal to 90% of the rated voltage): in the LV winding, it is 33.55 kW/51.96 kW; in the HV winding, it is 46.25 kW/71.63 kW; in the core, it is 63.8 kW/46.44 kW, and in constructive parts, it is 80 kW/120 kW; the overall sum is 383.22 kW/537.19 kW.

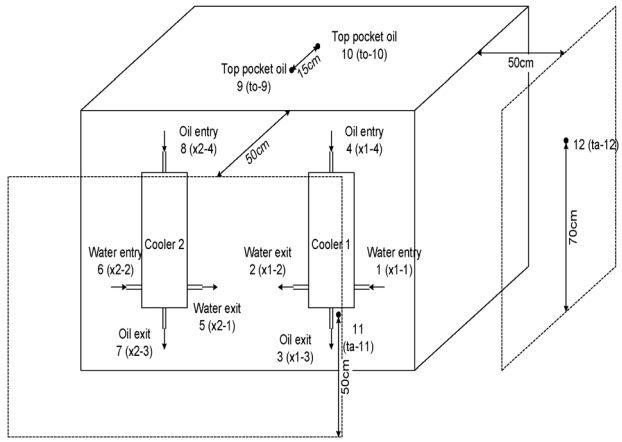

Fig. 4. Positions of PT100 sensors.

III. Experimental Determination of the Characteristics of Compact Coolers

As stated in the introduction, standard catalog data about the cooler were not available. For this reason, measurements on the transformer under real operation were made and used to determine the cooler properties required to be specified in the software [5].

The temperatures were measured outside the transformer tank (12 measuring points) at different loads. PT100 sensors were used (12 sensors). National Instruments' NI9217 measuring converter (four-wire measuring system) was used as a measuring device and Labview software was used for the acquisition of data on a laptop. The load (active power P (MW) and the reactive power Q (Mvar)) were obtained from a supervisory-control-and-data-acquisition (SCADA) system installed in the power station. The position of 12 PT100 sensors are shown in Fig. 4: 4 per each of the two coolers—entrance of water, exit of water, entrance of oil, and exit of oil: 2 for the top oil in pockets and 2 for the ambient temperature; sensor 11–50 cm from the tank wall, and 50 cm from the floor and sensor 12–50 cm from the tank wall and 70 cm from the floor.

Table I contains the results recorded in thermal steady states. The apparent power is given by $S = \sqrt{P^2 + Q^2}$. The values of the temperatures are steady-state values.

The data used for the determination of oil/water compact cooler properties: $\vartheta_{Hot\ Oil} = 47.92\,^{\circ}\mathrm{C}$, $\vartheta_{Cold\ Oil} = 43.99\,^{\circ}\mathrm{C}$, $\vartheta_{Cold\ Water} = 17.08\,^{\circ}\mathrm{C}$, $\vartheta_{Hot\ Water} = 31.51\,^{\circ}\mathrm{C}$, and cooling power 376 kW. Notes: 1) the ambient air temperature was 21.5 °C; 2) the temperatures were measured at nearly the rated current (99.11% of the rated current); 3) the losses were estimated as follows: $0.9911^2 \cdot 319.8\ \mathrm{kW} + 63.81\ \mathrm{kW} = 378\ \mathrm{kW}$; 4) due to cooling on tank surfaces, for the cooling power of the cooler, a value of 376 kW was adopted.

Thermal characteristics of oil (type Shell Diala D), given by producer, depending on oil temperature (ϑ), are: density $\rho(\mathrm{kg/m^3}) = 892 - 0.7\vartheta$, thermal conductivity $\lambda(\mathrm{W/(mK)}) = 0.12386 - 7 \cdot 10^{-5}\vartheta$, specific heat at constant pressure $c_P\ (\mathrm{J/(kgK)}) = 1912.9 + 4.4\vartheta$, volumetric thermal

TABLE I
MEASURED VALUES RECORDED IN THE STEADY STATES AT DIFFERENT LOAD STEPS (LS)

	LS 1 1 cooler	LS 2 1 cooler	LS 3 1 cooler	LS 4 1 cooler	LS 4 2 coolers
P (MW)	25.08	60.47	81.92	94.81	94.81
Q (Mvar)	8.44	12.00	13.78	28.89	28.89
S (MVA)	26.46	61.65	83.07	99.11	99.11
C1, OEn (°C)	–	–	–	–	39.16
C1, OEx (°C)	–	–	–	–	35.78
C1, WEn (°C)	–	–	–	–	16.59
C1, WEx (°C)	–	–	–	–	27.62
C2, OEn (°C)	31.00	38.82	42.69	47.92	38.81
C2, OEx (°C)	29.27	36	39.35	43.99	35.92
C2, WEn (°C)	17.02	16.87	16.8	17.08	16.97
C2, WEx (°C)	23.04	26.66	28.52	31.51	26.39
OTop1 (°C)	33.31	41.45	45.51	50.23	41.07
OTop2 (°C)	34.09	42.29	46.31	51.5	41.4
A1 (°C)	31.15	31.3	24.86	21.17	19.21
A2 (°C)	28.60	31.48	24.95	21.89	19.64

Key (for the temperature values): C—Oil to water compact cooler, O—Oil, W—Water, A—Air (during measurements with load step 1, air sensor 1 was on the sunny side and air sensor 2 in the shadow), En—Entrance, Ex—Exit, Top—Oil pocket on the tank cover

TABLE II
MAIN RESULT OF CALCULATIONS FOR THE RATED AND INCREASED LOAD

	Units	Rated load	Increased load
ϑ_{iw}	°C	17	25
ϑ_{ow}	°C	30.65	44.33
Oil flow	$\mathrm{m^3/h}$	187.8	202.7
Losses	kW	383.2	537.2
ϑ_{bo}	°C	44.64	63.05
ϑ_{ao}	°C	46.53	65.45
ϑ_{to}	°C	48.40	67.85
$\vartheta_{\mathrm{Cu\,a,\,HV}}$	°C	54.00	76.95
$\vartheta_{\mathrm{Cu\,a,\,LV}}$	°C	53.30	76.08
$(\vartheta_{\mathrm{Cu\,a}} - \vartheta_{\mathrm{ao}})_{\mathrm{HV}}$	K	7.48	11.50
$(\vartheta_{\mathrm{Cu\,a}} - \vartheta_{\mathrm{ao}})_{\mathrm{LV}}$	K	6.77	10.63
$\vartheta_{\mathrm{Cu\,hs,\,HV}}$	°C	62.03	88.25
$\vartheta_{\mathrm{Cu\,hs,\,LV}}$	°C	58.74	84.46
H_{HV}	–	1.82	1.77
H_{LV}	–	1.52	1.56
$\vartheta_{\mathrm{to,\,HV}}$	°C	47.81	67.35
$\vartheta_{\mathrm{to,\,LV}}$	°C	47.27	66.80

H—hot-spot factor, calculated as $(\partial_{\mathrm{Cu\,hs}} - \partial_{\mathrm{to}})/(\partial_{\mathrm{Cu\,a}} - \partial_{\mathrm{ao}})$
Indexing key:
Cu a—average winding temperature
Cu hs—hot-spot winding temperature
iw—temperature of the water entering the cooler
ow—temperature of the water exiting the cooler
bo—temperature of the oil exiting the cooler
ao—average temperature of the oil in the cooler
to—temperature of the oil entering the cooler
to, HV—temperature of the oil exiting HV winding
to, LV—temperature of the oil exiting LV winding
LV—low voltage winding
HV—high voltage winding

expansion coefficient $\beta(1/\mathrm{K}) = 0.7/892$, and kinematic viscosity $\nu(\mathrm{m^2/s}) = 10^{10^{0.252-0.007611\vartheta}}$. No eventual change in the thermal characteristics of the oil due to aging was considered.

The basic equation used for the determination of the oil flow through the oil/water compact cooler is

$$P_{\mathrm{Cooling}} = \rho\, Q_{\mathrm{Oil}} c_P (\vartheta_{\mathrm{HotOil}} - \vartheta_{\mathrm{ColdOil}}).$$

From the previous equation, an oil flow of $Q_{\mathrm{Oil}} = 189\ \mathrm{m^3/h}$ was calculated ($P_{\mathrm{Cooling}} = 376.3$ kW, $\vartheta_{\mathrm{HotOil}} = 47.92°\mathrm{C}$, $\vartheta_{\mathrm{ColdOil}} = 43.99°\mathrm{C}$, density determined at $\vartheta_{\mathrm{ColdOil}}$ and specific heat at $(\vartheta_{\mathrm{HotOil}} + \vartheta_{\mathrm{ColdOil}})/2$).

The rated pressure drop across the cooler was arbitrarily adopted (120 mbar) and afterwards, the pump was selected in a way to obtain a total oil flow equal to the value estimated from the measurements (189 $\mathrm{m^3/h}$) at the equilibrium state of the pressure (working point).

Similar to oil flow, the water flow was obtained from the results of measurements: $Q_{\mathrm{Water}} = 23.13\ \mathrm{m^3/h}$.

IV. RESULTS OF CALCULATIONS

A. Main Results of the Detailed THNM

Thermal calculations were made for two regimes: regime 1—rated power, rated voltage, and water temperature 17 °C, and regime 2—power higher by 12% than the rated power, voltage 90% of the rated voltage, water temperature 25 °C. A temperature of 17 °C was adopted as the water temperature during measurements (see Section III) and 25 °C was adopted as the maximum expected water temperature under the planned increased load.

Imperfect sealing of the transformer (oil leakage from the system supplying oil to the windings) was modeled by 20 openings, each with a diameter of 10 mm, in the oil distribution channel (the channel is between the entrance of oil to the tank and the holes supplying oil to the windings). Changes in the diameter and number of the openings in the oil distribution channel influenced the oil quantity for cooling non-OD-cooled elements (in the case of this transformer, only the core is non-OD cooled) and the cooling of the tank surfaces [6].

Table II shows the main results of the calculations: the characteristic temperatures of the oil and of the windings (hot-spot temperature and average winding temperature), the resulting hot-spot factor, and the characteristic temperature gradients.

From the obtained results, it is obvious that the temperatures at the rated load were very low, that is, much lower than allowed in the IEC Standard [2]. Observing top oil, it becomes clear that the low average winding and the winding hot-spot temperatures are a consequence of the oversized cooler—this was confirmed by the measurements presented in Table I for load step 4 (rated load, one cooler), when the temperature rise of the oil entering the cooler amounted to $47.92 - 17.08 = 30.84$ K, which is much lower than the allowed 60 K.

B. Discussion About the Hot-Spot Factor

1) Definition From IEC Standards: The employed software delivers detailed results enabling the identification of each influence relevant to the value of the hot-spot factor. IEC Standard 60076-2 [2] defines the hot-spot factor (H) as the product of factor Q, which describes the local increase of additional losses, and factor S, that describes nonuniform cooling (the variation in the liquid flow stream), that is, $H = Q \cdot S$.

2) Factor Q: In the considered case, the value of factor Q remains the same for the considered load conditions and is equal

to the ratio of losses (dc and additional) appearing in the conductor with maximum losses and the average value of the losses over all conductors of the winding: $Q_{\mathrm{LV}} = 1.493$ and $Q_{\mathrm{HV}} = 1.752$.

3) Value of Factor S: From the aforementioned values of factor Q and the hot-spot factor from Table II, based on the temperature of the oil entering the cooler, the following values are obtained ($S = H/Q$): $S_{\mathrm{LV}} = 1.018$ and $S_{\mathrm{HV}} = 1.039$ for the rated load and $S_{\mathrm{LV}} = 1.045$ and $S_{\mathrm{HV}} = 1.010$ for the increased load. Further text presents a detailed analysis of these factors, helping to understand the components influencing their values.

4) Influence of the Mixing of Hot Oil on Factor S: The temperatures of the oil exiting the windings are somewhat lower than those of the oil entering the cooler. The oil entering the cooler is a mixture of the oils exiting the windings, the oil exiting the core (in the considered example, the temperature of the oil exiting the core is somewhat higher—for the increased load, it amounts to 83.34 °C) and the bypass oil. This means that the real average oil temperature in the winding is lower than the one estimated from the mixed top oil. The following consequence is that the value of the hot-spot factor determined for the temperature of the oil in the winding would be different—for the example of increased load, the hot-spot factors would be $H_{\mathrm{LV}} = (84.46 - 66.80)/(76.08 - (66.80 + 63.11)/2) = 1.586$ and $H_{\mathrm{HV}} = (88.25 - 67.35)/(76.95 - (67.35 + 63.11)/2) = 1.783$. The corresponding S factors are $S_{\mathrm{LV}} = 1.062$ and $S_{\mathrm{HV}} = 1.018$ (the values obtained from the oil entering the cooler are $S_{\mathrm{LV}} = 1.045$ and $S_{\mathrm{HV}} = 1.010$).

5) Influence of Nonuniform Oil Velocity in the Radial Cooling Duct of a Zigzag Cooled Winding: Both windings (LV and HV) are zigzag cooled. In the LV windings, there are five axial conductors and six radial cooling ducts per pass and in the HV windings, there are four axial discs and five ducts (there are ducts between the oil washers and the discs). In the HV windings, there are more conductors in the radial direction (21, i.e., 22 conductors) and it is expected to have greater nonuniformity of the conductor temperatures. The width of all six axial cooling ducts (inner and outer axial ducts in each of the two layers of the LV windings and the inner and outer axial ducts in the HV windings) is 6 mm. The widths of the radial cooling ducts in the bottom and the top passes are presented in Table III for the LV winding and in Table IV for the HV winding. Using the LV winding as an example for an explanation of the deviations from the rated values: the reduction from 4 to 3.6 mm originates from the shrinkage of the spacer by 7% (0.074 =0.28 mm) and the shrinkage of the insulation by 20% ($0.2 \cdot 0.6\mathrm{mm} = 0.12$ mm); the reduction from 3.6 to 2.329 mm originates from the bulging effect; the length of the axial duct in the zone of the conductor was taken to be equal to the rated conductor height (without any effects of pressing or bulging). Empirical rules are used for the estimation of bulging. These yielded higher values of bulging for a CTC type of conductor (LV winding) than for a flat conductor (HV winding). The calculation method considers all quoted nonuniformities, those in the size of ducts and those of different number of conductors in radial direction (21, that is, 22 in the HV disc winding).

TABLE III
WIDTH (in mm) OF THE RADIAL COOLING DUCTS FROM THE BOTTOM IN THE BOTTOM AND TOP PASSES OF THE LV WINDINGS

	Rated	Shrunk	Hydraulic
Ducts in the bottom pass			
1	2	1.8	1.164
2	4	3.6	2.329
3	4	3.6	2.329
4	4	3.6	2.329
5	4	3.6	2.329
6	2	1.8	1.164
Ducts in the top pass			
1	2	1.8	1.164
2	4	3.6	2.329
3	4	3.6	2.329
4	4	3.6	2.329
5	4	3.6	2.329
6	4	3.66	3.024

TABLE IV
WIDTH (in mm) OF THE RADIAL COOLING DUCTS FROM THE BOTTOM IN THE BOTTOM AND TOP PASSES OF THE HV WINDINGS

	Rated	Shrunk	Hydraulic
Ducts in the bottom pass			
1	3	2.79	2.61
2	6	5.58	5.22
3	7	6.51	6.15
4	5	4.65	4.29
5	3	2.79	2.61
Ducts in the top pass			
1	3	2.79	2.61
2	5	4.65	4.29
3	7	6.51	6.15
4	3	2.79	2.43
5	3	2.79	2.61

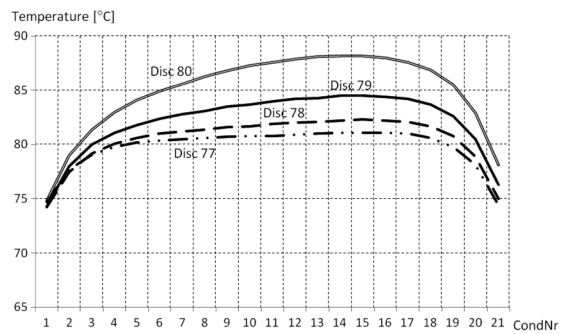

Fig. 5. Distribution of the conductor temperatures in the top pass of the zigzag-cooled HV winding.

Figs. 5 and 6 show the distribution of the conductor temperatures in the HV windings: in the top pass (top four discs; disc number 80 is at the top of the winding) (Fig. 5) and in the bottom pass (bottom 4 discs; disc number 1 is at the bottom of the winding) (Fig. 6).

The highest temperatures appear in the discs with the highest losses (disc 1 in the bottom pass and disc 80 in the top pass). In addition to the losses, the factor influencing the distribution of temperatures over conductors is the distribution of oil flow over radial cooling ducts. Fig. 7 shows the distribution of these oil

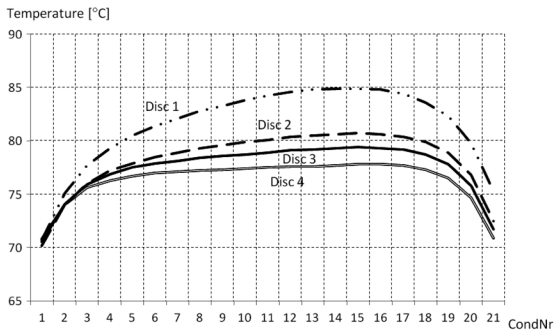

Fig. 6. Distribution of the conductor temperatures in the bottom pass of the zigzag-cooled HV winding.

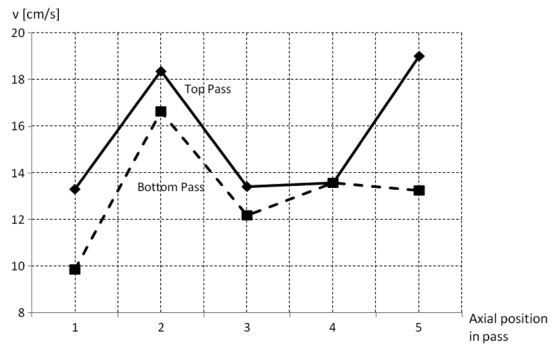

Fig. 7. Distribution of the oil velocity in radial cooling ducts of the first (bottom) and the last (top) passes of the zigzag-cooled HV winding.

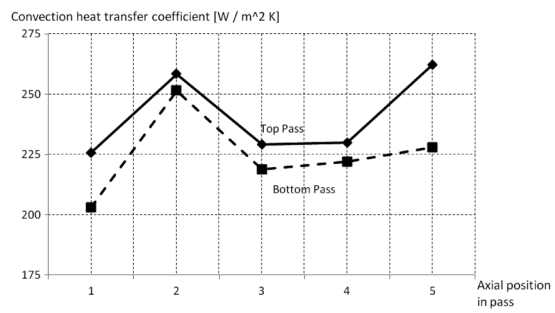

Fig. 8. Average convection heat-transfer coefficients in the radial cooling ducts of the bottom and the top passes of the zigzag-cooled HV winding.

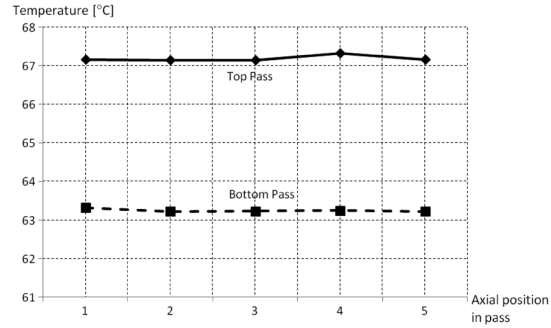

Fig. 9. Average oil temperature in radial cooling ducts of the bottom and top passes of the zigzag-cooled HV winding.

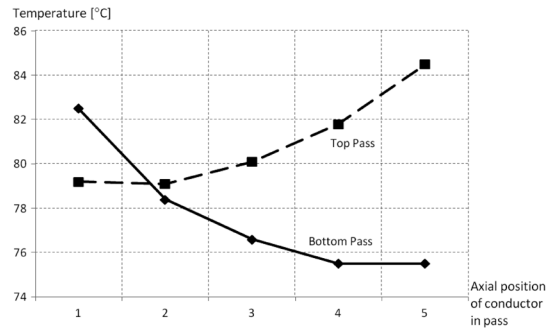

Fig. 10. Distribution of the conductor temperatures in the top and bottom passes of the zigzag-cooled inner layer of the LV winding.

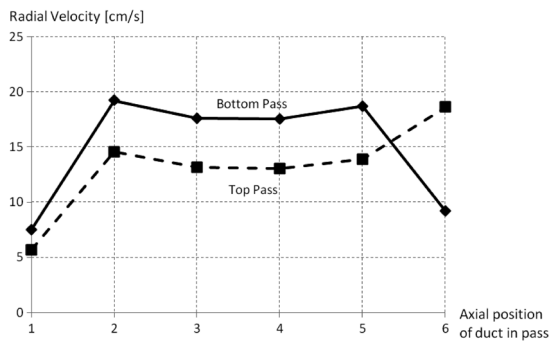

Fig. 11. Distribution of the oil velocity in the radial cooling ducts of the bottom and the top passes of the zigzag-cooled inner layer of the LV winding.

velocities in the bottom and top passes, obtained by solving the hydraulic network presented in [5].

Fig. 8 presents the average convection heat-transfer coefficients in each of the radial ducts and Fig. 9 shows the average oil temperature in each radial duct). The values of the convection heat-transfer coefficients and oil temperatures near the conductors were used in the equations corresponding to the thermal network [5] to calculate the temperature of the conductors.

Similar results as those for HV in Figs. 5–7 are given for the inner layer of the LV windings; the highest temperatures appear at the top conductor of the top pass and the bottom conductor of the bottom pass, since the highest losses are there (see Fig. 3); the additional losses at the bottom and the top of the windings are much higher in the inner layer than in the outer layer and, consequently, the temperatures are higher in the inner layer. Fig. 10 shows the distribution of the conductor temperatures in the top pass and in the bottom pass (numbering of the conductors in the pass is from the bottom; there is only one conductor in the radial direction). Fig. 11 shows the distribution of oil velocities in the bottom and top passes.

6) Quantification of the Nonuniformity in One Pass: The factor S given in Section IV-B-5 follows the definition, but the influence of the nonuniform distribution of the oil flow in the radial ducts on the distribution of the conductor temperature could be better observed by considering only one pass. Table V contains the local hot-spot factors for the bottom pass and for the top pass of the HV winding; these hot-spot factors are defined as the hot-spot factor for a complete winding (expression below Table II), where the values of the temperature of the hottest conductor in the pass, average temperatures of conductors in the pass, and oil entering and oil exiting the pass were used.

The H_{LP} and Q_{LP} factors calculated locally for the bottom and the top passes were smaller than their values for the entire HV winding (1.77 for H, see Table II, and 1.752 for Q, see

TABLE V
CALCULATED VALUES OF LOCAL HOT-SPOT FACTORS IN THE HV WINDING WITH THE INCREASED LOAD

		Bottom Pass	Top Pass
ϑ_{boP}	°C	63.11	67.05
ϑ_{toP}	°C	63.37	67.35
$\vartheta_{Cu\,a\,P}$	°C	78.34	81.79
$\vartheta_{Cu\,hs\,P}$	°C	84.9	88.2
H_{LP}		1.426	1.429
Q_{LP}		1.364	1.380
S_{LP}		1.045	1.036

Section IV-B-2). This is a consequence of "averaging" the losses over the entire winding: the maximum losses in the conductors remain the same, while average losses over the conductor drop if the entire winding is considered instead of the bottom or top pass. The factor S_{LP} changes slightly with respect to the value for the entire winding (1.01, see Section IV-B-3). The number of radial ducts per pass and widths of the ducts in this transformer are well designed. The detailed THNM enables the calculation of the distribution of oil in the radial ducts and, thus, to check the values of hot-spot temperature and the corresponding H_{LP} and S_{LP} factors; the most critical is the design of the passes at the top and bottom of the winding, where the highest eddy losses appear. Many radial ducts per pass or variable width of ducts can cause low radial velocities in some of the ducts, a high value of the S factor, a high hot-spot temperature, and damage to the adjacent conductor.

7) Conclusions: It could be concluded that the S factor depends on numerous factors and can be derived only using detailed thermal-hydraulic calculations. It is also important to note that S factor changes; for case study transformer, it has been shown that S factor changes with the load (see IV-B-3)). This is a consequence of changing the hydraulic resistances, caused by the change of viscosity, being extremely temperature dependent. Bigger change of S factor can be expected in different cooling modes of the same transformer, for example, oil directed air forced (ODAF) or oil natural air forced (ONAF) cooling. The above mentioned dependence of the hydraulic resistances on the losses, oil temperature and viscosity implies that the S factor depends on the distribution of the losses in the winding, meaning, in fact, that the S and Q factors are not decoupled. Nevertheless, the strongest argument that the concept of S and Q factors is not particularly meaningful is that the S factor, in fact, does not describe non-uniformity of the cooling since the position of the highest losses and the position of the worst cooling can differ and multiplying the S and Q factors, defined as the ratios of the highest to average temperatures caused by non-uniform losses and non-uniform cooling, respectively, would lead to a too high hot-spot factor.

C. Note About Improving the Accuracy of Calculation

The distribution of losses in windings was determined by assuming that the temperature at all conductors is constant and equal to 75 °C (for both operating conditions—rated load and planned increased load). More accurate values of the losses in each conductor would be obtained starting from the values of the calculated axial and radial components of the magnetic field at the positions of each conductor and calculating the losses in each conductor based on the electrical resistivity, which depends on the temperature of the conductor; and the dc losses were calculated using the elementary equation for resistance calculation $R = \rho l/S$).

TABLE VI
RESULTS OF THE CALCULATIONS PERFORMED AFTER OMITTING THE BARRIERS IN THE LV/HV WINDINGS

		Original	Changed LV	Changed HV
Total oil flow	m^3/h	187.6	188.5	188.8
Flow through LV	m^3/h	26.35	28.85	24.37
Flow through HV	m^3/h	29.21	27.34	32.02
$\vartheta_{Cu\,a,\,LV}$	°C	53.30	53.84	53.48
$\vartheta_{Cu\,hs,\,LV}$	°C	58.74	60.01	59.05
H_{LV}		1.52	1.62	1.53
S_{LV}		1.018	1.085	1.025
$\vartheta_{Cu\,a,\,HV}$	°C	54.00	54.28	56.29
$\vartheta_{Cu\,hs,\,HV}$	°C	62.03	62.54	62.98
H_{HV}		1.82	1.82	1.49
S_{HV}		1.039	1.039	0.850

V. INFLUENCE OF A CHANGE OF THE BARRIERS ON THE S FACTORS

As an illustration, the calculations were run after changing the construction of the winding. (The results are presented in Table VI.)

The first change with respect to the original construction was omitting the barriers in the LV winding. In the original construction, there were 21 barriers, that is, there were 20 zigzag oil passes, each containing six ducts (2 radial ducts of 2 mm near the barriers and 4 radial ducts of 4 mm between each of the five conductors in the axial direction). After the change, there was one pass of the 11 ducts at the bottom of the winding and 6 passes of the 16 ducts; barrier nos. 2, 4, 5, 7, 8, 10, 11, 13, 14, 16, 17, 19, and 20 counted from the bottom were omitted (two 2-mm ducts and 1-mm-thick barrier were replaced by a radial duct of 5 mm).

The second change with respect to the original construction was omitting the barriers in the HV winding. This was realized in a similar way—instead of 20 passes with five radial ducts each, there was one pass with nine ducts (at the bottom) and six passes with 13 ducts.

As expected, the reduction in the number of barriers reduced the hydraulic resistance and finally led to an increase in the oil flow through the windings where this change had been realized. The slight increase of the flow in the winding with the smaller number of barriers improved the cooling of the winding, but this effect was less than the effect of the reduction of oil velocities in each of the increased number of parallel radial ducts: the reduction of the number of barriers in the end led to an increase of the average and hot-spot temperatures. The most extreme change appears in the hot-spot factor and the S_{HV} factor after reducing the number of barriers in the HV winding: S_{HV} decreased to below 1. This is a consequence of the distribution of oil flow in the radial ducts. Fig. 12 presents the distribution in the last (top) pass—contrary to the original construction, where there was no big difference in the oil velocities over five radial ducts in the top pass (see Fig. 7), the oil velocity in the radial duct around

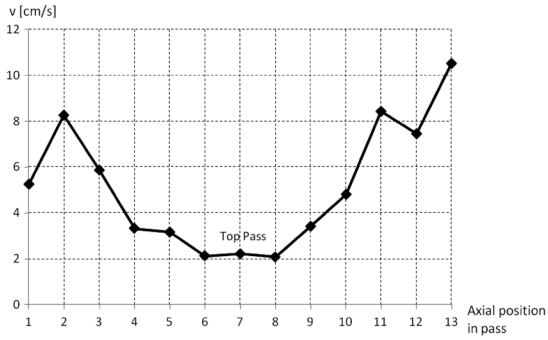

Fig. 12. Distribution of the oil velocity in the radial cooling ducts of the top pass of the zigzag-cooled HV winding after a reduction of the number of barriers.

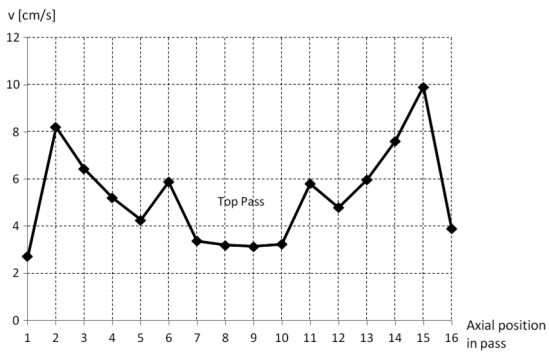

Fig. 13. Distribution of the oil velocity in the radial cooling ducts of the top pass of the inner layer of the zigzag-cooled LV winding after reduction of the number of barriers.

the top disc (ca. 7.5 and 10.5 cm/s) was much higher than in radial ducts in the middle of the pass (ca. 2 cm/s). This effect did not appear in the LV winding after increasing the number of radial ducts in one zigzag pass (see Fig. 13). It is obvious that the final result of oil distribution over the ducts in one pass depends on the width and the length of the ducts—application of the detailed THNM (optionally computational fluid dynamics (CFD) methods) could be employed to determine the distribution of oil flow for any assumed construction.

VI. Recommendations About the Possibility of Increasing the Load

According to [4], the estimated accuracy of the applied calculation method is 3 K for the oil and 5 K for the winding temperature. In [7], a comparison of the calculated and measured temperatures was published using, as an example, a 750-MVA ODAF transformer, and the accuracy was briefly discussed. The reliability of the method was subsequently checked on 15 transformers of different ratings from four different producers (some of them equipped with fiber-optic temperature sensors, for example: 40 MVA (ONAF, 13.8/132 kV), 300 MVA (ONAF, 138(69)/420 kV), 330 MVA (ODAF, 220/380 kV), 502 MVA (ONAF, 115/380 kV), and 752 MVA (ONAF, 230/380 kV); the specification of the power was given for the power in the most intense cooling mode; cooling modes foreseeing the possibility of switching off the pumps and/or switching off fans were also calculated).

Standard [3] (loading guide) specifies the limits for the loading of a transformer. For a normal cyclic load, the limits for large power transformers (more than 100 MVA) are: hot-spot temperature 120 °C, top oil temperature 105 °C and a maximum current load of 1.3 p.u. The top-oil temperature by the planned increased load (67.85 °C) was much lower than the allowed value. The temperature of the hot spot of the HV winding, which is higher than the hot spot of the LV winding, amounted to 88.2 °C; after adding a safety margin of 5 K, one obtains 93.2 °C, which is below the allowed limit of 120 °C [3]. According to standard [3], the value at which aging of insulation is considered as normal is 98 °C for thermally nonupgraded paper and 110 °C for thermally upgraded paper. The hot-spot temperature of 93.2 °C is below 98 °C, meaning that the target increased load of the transformer is also acceptable as long-term loading.

Since the hot-spot temperature approached the allowed limits, pollution of the coolers becomes an important issue [21], that is, the coolers should be cleaned regularly—the temperature of oil entering the cooler (hot oil) and/or oil exiting the cooler (cold oil) should be monitored and the coolers cleaned if high values of these temperatures (roughly an increase of 5 K with respect to the clean state) are detected.

The calculated oil velocity in the HV winding was quite high—in the axial cooling duct, it was 57 cm/s with one cooler and the pump in operation. Typically, the assumed velocity under which the generation of static electricity commences is 1 m/s, but designers try to keep the maximum velocity of the oil in the winding below 50 cm/s. Consequently, it is not recommended to run both pumps and coolers.

Finally, the recommendation is to check the tank heating (using thermal imaging) due to a higher leakage flux in case of increased load (112 MVA); it should be noted that for the determination of the leakage flux distribution (and consequent losses in the constructive parts of a transformer and the heating of these parts), special FEM calculations are required [22]–[25] and it is not an issue covered by the detailed thermal-hydraulic model. The situation is similar for the bushings, cable-end connections, and leads, which have not been checked—the maximum current overload amounts to 24.4%, being smaller than the allowed 30% overload of large power transformers in the normal cyclic load mode [3]; since these elements have a small thermal inertia, it was assumed that they are sized to withstand an overload of 30%.

The results of thermal analyses indicated that the considered transformer would be inside the thermal limits defined in the transformer loading guide [3] and could operate with increased load without any reconstruction of the transformer.

VII. Conclusion

This paper presents the application of the THNM model and corresponding design software to the practical problem of the estimation of the feasibility of increasing the load of a 100-MVA oil power transformer with directed oil flow and water compact coolers. In transformer engineering practice, large safety margins are introduced due to the limited accuracy of the calculation methods and tools. The consequence is that transformers are oversized (the real rated power is higher than the declared

rated power) and there is a possibility to load them beyond their declared rated power. An estimation of the possibility of increasing the load requires repeated accurate thermal calculations—state-of-the art methods are FEM calculation tools for the distribution of power losses in the windings and a detailed THNM for the temperatures. This paper describes practical details of the application of such calculations in the considered project, with a final recommendation of whether the load could be increased with/without intervention of the examined transformer.

This paper contains a numerical analysis of the hot-spot factor, thus contributing to a better understanding of phenomena influencing this factor: the difference in the oil temperatures exiting the windings and the nonuniformity of the losses and cooling over the windings. The detailed THNM for the complete transformer enabled such decomposition by virtue of the solid physical base of the model. As a consequence, the detailed and integrated THNM of the complete transformer offered not only the determination of the position and temperature of the hot spot, but was also a good basis for the detection of potential weak points in the design and their correction (the model responds to changes in any detail of the construction).

Our final conclusion is that calculating the hot-spot factor as the product of two independent factors (Q, describing nonuniformity of the losses over winding, and S, describing nonuniformity of the cooling) is not a good approach. The reasons are: 1) the S and Q factors are not decoupled, that is, the S factors cannot be calculated assuming a uniform distribution of the losses; 2) the highest losses and the worst cooling can appear at different positions and if the Q factor would be defined as the factor of the nonuniformity of losses and the S as the factor of nonuniform cooling (assuming uniform losses), the final hot-spot factor would be too high; 3) omitting barriers in the HV winding in the studied example reduced the S factor, even though the change in the oil-flow stream resulted in poorer cooling. Thus, the S factor is of no particular meaning when comparing various designs. Instead of this, the hot-spot factor should be determined based on the distribution of the conductor temperatures, obtained from a detailed THNM, where the losses in each conductor (or the values of axial and radial magnetic fields at the position of each conductor) are input data. The software employed in this paper accurately covers hydraulic and thermal issues. Regarding the losses, details to improve the state-of-the-art calculation methods used and described in this paper were indicated.

REFERENCES

[1] P. S. Georgilakis, *Spotlight on Modern Transformer Design*. New York, USA: Springer, 2009.

[2] *Power Transformers—Part 2: Temperature Rise for Liquid-Immersed Transformers*, IEC 60076-2 ed. 3.0, Feb. 2011.

[3] *Loading Guide for oil-Immersed Power Transformers*, IEC 60076-7, Dec. 2005.

[4] Z. Radakovic and M. Sorgic, "wirtschaftliche betrachtung der thermischen auslegung von ölgekühlten leistungstransformatoren," in *Elektrizitätswirtschaft 107*, 2008, pp. 32–38, Heft 15.

[5] Z. Radakovic and M. Sorgic, "Basics of detailed thermal-hydraulic model for thermal design of oil power transformers," *IEEE Trans. Power Del.*, vol. 25, no. 2, pp. 790–802, Apr. 2010.

[6] M. Sorgic and Z. Radakovic, "Oil-forced versus oil-directed cooling of power transformers," *IEEE Trans. Power Del.*, vol. 25, no. 4, pp. 2590–2598, Oct. 2010.

[7] Z. Radakovic, M. Sorgic, W. V. d. Veken, and G. Claessens, "Ratings of oil power transformer in different cooling modes," *IEEE Trans. Power Del.*, vol. 27, no. 2, pp. 618–625, Apr. 2012.

[8] M. Yamaguchi, T. Kumasaka, Y. Inui, and S. Ono, "Flow rate in a self cooled transformer," *IEEE Trans. Power App. Syst.*, vol. PAS-100, no. 3, pp. 956–963, Mar. 1981.

[9] W. V. d. Veken, J. Declercq, M. Baelmans, and S. V. Mileghem, "New perspectives to overloading with accurate modeling of thermal transient in oil-immersed power transformers," in *Proc, IEEE/Power Eng. Soc. Transm. Distrib. Conf. Expo.*, 2001, vol. 1, pp. 147–152.

[10] F. P. Incropera and D. P. DeWitt, *Heat and Mass Transfer*, 5th ed. Hoboken, NJ, USA: Wiley, 2002.

[11] I. E. Idelchik, *Handbook of Hydraulic Resistances*. Boca Raton, FL, USA: CRC, 1994.

[12] *VDI-Gesellschaft Verfahrenstechnik und Chemieingenieurwesen (GVC)*. Berlin, Germany: Springer-Verlag, 1997, Auflage, VDI Wärmeatlas.

[13] C. O. Olsson, "Prediction of nusselt number and flow rate of buoyancy driven flow between vertical parallel plates," *J. Heat Transfer*, vol. 126, no. 1, pp. 97–104, 2004.

[14] A. Weinläder, W. Wu, S. Tenbohlen, and Z. Wang, "Prediction of the oil flow distribution in oil-immersed transformer windings by network modelling and computational fluid dynamics," *IET Elect. Power Appl.*, vol. 6, no. 2, pp. 82–90, 2012.

[15] C. Sang Moon and K. Joong-Kyoung, "Prediction and evaluation of the cooling performance of radiators used in oil-filled power transformer applications with non-direct and direct-oil-forced flow," *Exp. Thermal Fluid Sci.*, vol. 44, pp. 392–397, 2013.

[16] F. Torriano, M. Chaaban, and P. Picher, "Numerical study of parameters affecting the temperature distribution in a disc-type transformer winding," *Appl. Thermal Eng.*, vol. 30, pp. 2034–2044, 2010.

[17] P. Picher, F. Torriano, M. Chaaban, S. Gravel, C. Rajotte, and B. Girard, "Optimization of transformer overload using advanced thermal modelling," in *Proc. CIGRE Conf.*, Paris, France, 2010, A2-305.

[18] M. T. Villén, J. Letosa, A. Nogués, and R. Murillo, "Procedure to accelerate calculations of additional losses in transformer foil windings," *Elect. Power Syst. Res.*, vol. 95, pp. 85–89, 2013.

[19] S. V. Kulkarni and S. A. Khaparde, *Transformer Engineering: Design, Technology, Diagnostics*. Boca Raton, FL, USA: CRC, 2012.

[20] CIGRE Working Group A2.38, "Transformer thermal modelling, working version of the brochure," internal document, to be published.

[21] Z. Radakovic and A. Popovic, "Variation of steady-state thermal characteristics of transformers with OFWF cooling in service," *Elect. Power Compon. Syst.*, vol. 31, no. 8, pp. 817–829, 2003.

[22] T. R. Bott, *Fouling of Heat Exchangers*. New York, USA: Elsevier, 1995.

[23] J. Turowski and A. Pelikant, "Eddy current losses and hot-spot evaluation in cover plates of power transformers," *Proc, Inst. Elect. Eng. Elect. Power Appl.*, vol. 144, no. 6, pp. 435–440, 1997.

[24] K. Dong-Hun, H. Song-Yop, and K. Sang-Young, "Improved design of cover plates of power transformers for lower eddy current losses," *IEEE. Trans. Magn.*, vol. 35, no. 5, pp. 3529–3531, Sep. 1999.

[25] E. Schmidt and P. Hamberger, "Design optimization of power transformers Part 2—Eddy current analyses for tank wall and core clamping parts," in *Proc. Int. Conf. Power Syst. Technol.*, Singapore, 2004, pp. 21–24.

Zoran Radaković, photograph and biography not available at the time of publication.

Uroš Radoman, photograph and biography not available at the time of publication.

Predrag Kostić, photograph and biography not available at the time of publication.